DETERMINING THE CAUSE OF BEARING FAILURES IN CIRCULATING WATER PUMP MOTORS

by

Julia Postill

Mechanical Engineer

Turbo Components and Engineering

Houston, Texas

Malcolm E. Leader

Consultant

Applied Machinery Dynamics

Dickinson, Texas

Ray D. Kelm

Owner

Kelm Engineering

Angleton, Texas

and

Chesley Brown

Senior Engineer

TXU, CPSES

Glen Rose, Texas

Julia Postill is a Mechanical Engineer at TCE/Turbo Components & Engineering, in Houston, Texas. At TCE she specializes in fluid film bearing design and analysis, seal design, rotor bearing system dynamics, troubleshooting, and failure analysis. Mrs. Postill has been with TCE since October 1998. Prior to joining the Turbo Components & Engineering team, she worked as a design engineer for an aftermarket bearing manufacturer for 7fi years. Before that she worked as a Scientific Research Engineer in ICSITMFS, a design institute in Bucharest, Romania.

Mrs. Postill received her BSME (1980) from the Polytechnic Institute of Bucharest, Romania. She has participated in writing several technical papers. She is a registered Professional Engineer in the State of Texas and a member of the Houston Chapter of the Vibration Institute, ASME, and STLE.

Malcolm E. Leader is a Turbomachinery Consultant and Owner of Applied Machinery Dynamics, in Dickinson, Texas. He is currently involved in the design, testing, modification, and installation of rotating equipment. He spends time doing theoretical design audits and working in the field implementing changes and overseeing installations.

Mr. Leader obtained his B.S. (1977) and M.S. (1978) degrees from the University of Virginia. While there, he worked extensively on experimental rotordynamics and hydrodynamic bearing design. He has written several papers on the subjects of experimental rotordynamics, bearing design, design audits for rotating equipment, and practical implementation of rotordynamic programs. Mr. Leader is a member of ASME, Sigma Xi, the Houston Chapter of the Vibration Institute, and is a registered Professional Engineer in the State of Texas.

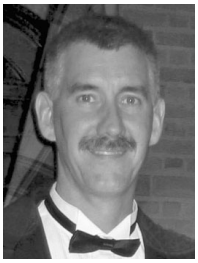

Ray Kelm is the Owner of Kelm Engineering, in Angleton, Texas. His primary duties involve numerical modeling and field testing of dynamic systems including rotating, reciprocating, and static machinery. He has 21 years' experience in the petrochemical and engineering consulting businesses.

Mr. Kelm received a BSME (1983) from Texas A&M University, and an M.S. degree (Mechanical and Aerospace Engineering) from the University of Virginia. He is member of ASME and the Vibration Institute, and is a Category VI ISO certified vibration specialist.

ABSTRACT

Eight vertical circulating water pumps are used to circulate condenser water at the generation station in a nuclear power plant. The pump installation is pictured in Figure 1. The motor pump system is arranged vertically with the drive motor above the pump. Each pump is driven by a 28-pole, 2500 hp synchronous motor at 271 rpm. The motors sit on a platform that projects out over a large reservoir and each one delivers 275,000 gpm at about 12 psig. The pumps are located below the motors in the reservoir. There are four pumps per generating unit. Each unit can run at full capacity with three pumps. With two pumps out of service the generating capacity drops about 10 percent. Three lower motor bearing failures occurred shortly after sudden ambient temperature drops. Analysis showed that there was adequate lubrication but the original bearing design was very sensitive to clearance. A finite element analysis of

the motor proved that the case would pinch the bearing when cooled from 70°F to 25°F. This reduced the bearing clearance significantly and caused the failures. A new profiled bearing was developed that would provide better rotor support with larger clearances that would be more tolerant of thermal clearance changes.

Figure 1. Installation at Power Plant.

The bearing failure analysis was wide in scope and was conducted by a large team including engineers from the power plant, turbomachinery consultants, repair shops, and bearing manufacturers. Many different theories were considered and investigated. This paper examines the investigations of the bearing lubrication with a computational fluid dynamics (CFD) analysis, the motor rotordynamics, the effects of ambient temperature drop, and the manufacture of a new bearing design.

BACKGROUND

The initial incident was a forced outage due to the failure of a lower motor guide journal bearing in one of the motors. The lower motor bearing is opposite the thrust end. Up until November 2001, the eight circulating water pumps had been operating for at least eight years without experiencing any failures of the lower guide bearings. Eventually, there was a total of three identical failures of the lower motor bearings.

The first bearing failure occurred on November 29, 2001. The lower motor guide journal bearing on unit 2-02M indicated a temperature spike in the bearing metal thermocouple of over 300°F. This happened just after a sudden drop in ambient air temperature caused by a cold front passing through the area. The motor was removed and refurbished and returned to service about January 28, 2002. It ran for about three days and then the lower guide bearing again indicated a bearing metal temperature spike of 300°F following another drop in ambient air temperature. The stator winding temperatures also dropped from 230°F to 200°F just prior to the spike. The third lower bearing failure occurred on unit 2-03M on February 26, 2002, after 12 months of operation following a major overhaul.

LOWER BEARING DESCRIPTION

The standard original equipment manufacturer (OEM) lower bearing is 16 inches in diameter and 3.4 inches long. It has a circular bore divided by six axial grooves. It was designed to run with tight clearances to assure low vibration. There are two circumferential grooves located at the ends of the bearing load supporting area. The one on the bottom is designed to supply oil and the one on the top is designed to drain the oil. There are two oil-pumping holes diametrically opposite into the rotating sleeve that are designed to match their axial location with the oil supply groove in the bearing. There is a drain hole that connects the drain groove with the oil tank.

FLOW MODELING OF THE MOTOR BEARING

Numerical models of the fluid flow passages of the oil sump and the bearing liner were developed using computational fluid dynamics software. The basic model is shown in Figure 2.

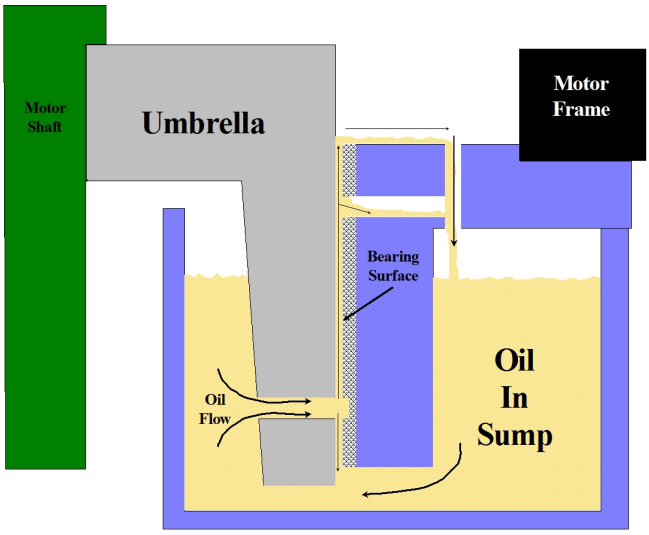

Figure 2. Cross Section of Lower Motor Bearing.

The lower motor bearing journal is an "umbrella" shaped attachment to the shaft. An oil bath sump is used to submerge the lower half of the journal. Two diametrically opposed ½ inch pumping holes use the velocity differential to force oil into a circumferential groove in the babbitt. Oil fills this groove and is forced upward to the top of the bearing where it spills into another groove that is connected to two ¾ inch drain pipes back to the sump. Various conditions could exist that would adversely curtail proper oil delivery. The factors that the CFD analysis evaluated were:

- Alignment of the pumping hole with the distribution groove.
- Oil level in the sump.
- Oil viscosity and temperature.

Figure 2 is a depiction of the free surface model of the sump, rotating umbrella assembly, and the inlet to the pumping tube. The purpose of this model was to determine the quality of the oil inlet conditions at the pumping tube and to evaluate the sensitivity of the oil flow to the height of the oil in the sump and the sensitivity to varying sump oil temperature.

The free surface model involves a two-fluid model of the sump including the oil in the sump with a vented air volume above the liquid. The free surface model is an axisymmetric, single element thickness model. Boundary conditions include rotation on the inside and bottom of the umbrella, nonslip walls at all other wall locations, and an average inlet velocity into the pumping tubes of 0.233 in/sec (0.00592 m/s); the average velocity is based on a calculated total oil flow of 1.3 gpm at 120°F.

The free surface model produced very useful information. The primary insight was that the pumping tubes must be well aligned with the lower circumferential bearing groove if the pumping action is to be efficient. Misalignment of the tube to groove by half the tube diameter will reduce the volume of oil flow by 10 to 15 percent, which could starve the upper half of the bearing especially if the oil viscosity were high at the time.

The oil level in the sump, which controls the head seen by the oil pumping tubes, was varied by plus and minus a half inch with little effect. Therefore, it was concluded that slight variations in oil sump level that had been observed were not related to the failures.

It was also found that the oil viscosity as related to temperature was significant. Figure 3 plots the pressure and flow as a function

of temperature. The low temperature section of the plot is extrapolated data.

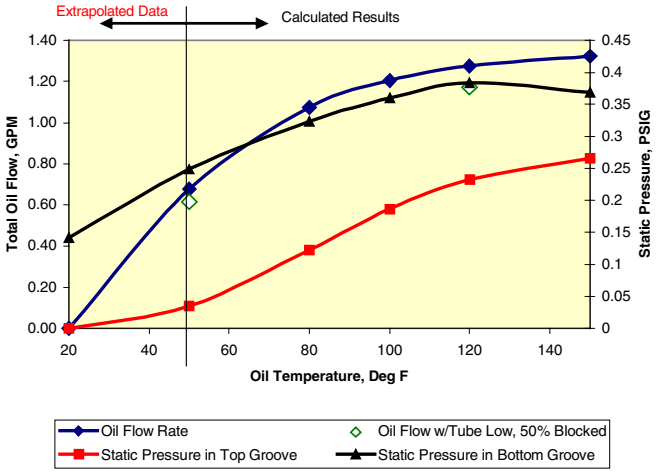

Figure 3. Flow and Pressure as a Function of Temperature.

It is believed that the sump temperature would never drop below 50°F in operation, assuring adequate lubrication. However, if a motor were started after having sat idle at temperatures below freezing, the lubrication would be marginal or inadequate.

A three-dimensional flow model, Figure 4, of the sump was made including pumping tubes, bearing liner, and drain tube while excluding the free surface model in the sump. Exclusion of the free sump model was done to make the numerical solution practical and was confirmed to be a valid modeling assumption. The fluids in these models are air and heavy medium (VG 68) oil. The temperature-dependent fluid properties are used for the oil. For all cases, the bearing film thickness was modeled to be 9 mils on diameter.

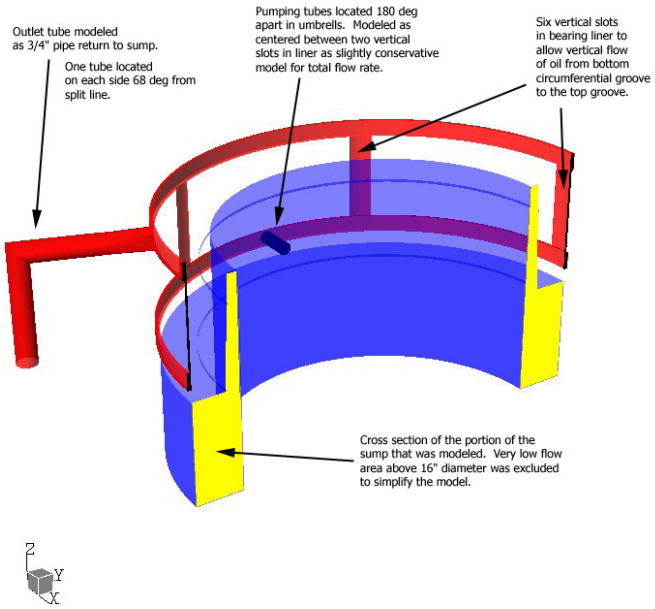

Figure 4. CFD Three-Dimensional Model of Lower Motor Bearing.

The primary result of this analysis was to examine the flow velocities and look for areas that had entrained air or might be starved for oil. The entrained air was found to be less than 3 percent by volume. Figure 5 shows that the oil velocities in the grooves are caused by rotation of the umbrella journal and there is good flow up through the axial grooves and out the drains.

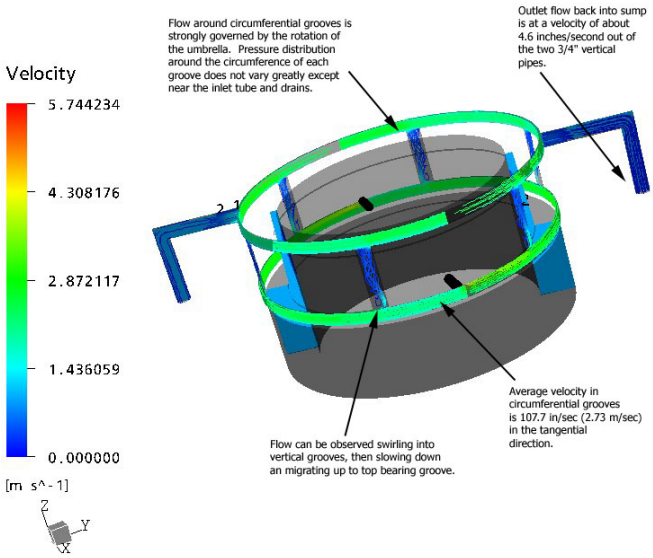

Figure 5. CFD Calculated Oil Velocities.

PLAIN BEARING ANALYSIS

At the time the rotordynamics analysis was done, the reasons for the bearing failure were not clear. The failure pattern looked like a rub had developed in the upper half of the bearing, which is why the lubrication method came under such scrutiny. The OEM set clearance on these bearings was in the ½ mil-per-inch diameter range. This is considered very tight and would not be used in a horizontal mounted machine. In a vertical orientation, the bearing must produce sufficient support for the rotor to withstand imbalance forces and transient loads. The analysis indicated that the tight bearing was necessary when a plain circular design was chosen. A new design was proposed with preloaded pads that would provide adequate rotor support with much larger clearances. This way, any clearance reduction due to thermal effects would not cause rubs and bearing failures. For even more support, an offset taper pad arrangement was considered, but these units routinely operate in reverse rotation since there are no check valves in the discharge lines. The pumps run backwards up to 250 rpm before they are started, therefore a symmetrical bearing design was necessary.

Theoretically, an unloaded circular bushing has virtually no direct stiffness. In order to account for the geometric asymmetries observed in samples, a slight preload was applied to the geometry of the original bearing for analysis. Figure 6 shows that this does lead to some direct stiffness that increases as the clearance decreases. At 8 mils diametral clearance the direct stiffness is less than 1000 pounds per inch, which is the same as 1 pound per mil—insignificant. At greater clearances, the direct stiffness continues to drop.

Direct damping is what makes the original design work and this is plotted as a function of clearance in Figure 7. This shows that the tighter the clearance, the more direct damping is produced by the oil film. However, we know from experience that set clearances below 8 mils are not likely to survive a drop in ambient temperature due to a cold front.

REDESIGNED BEARING ANALYSIS

The bearing redesign had as its major objective to provide good lateral rotor support with increased clearance. The increased clearance is necessary to allow for thermal distortion from ambient temperature drop. The easiest and most common way to do this is with a "profiled" bearing design. Profiled means that the radius of curvature of the bearings pads is not concentric with the geometric center of the rotor journal. In bearing terms, this creates preload from a converging-diverging oil film on the bearing surface. As the

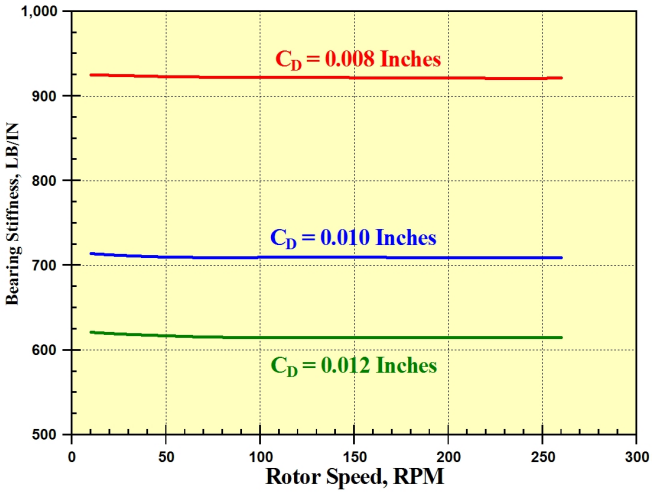

Figure 6. Plain Bearing Stiffness Versus Speed and Clearance.

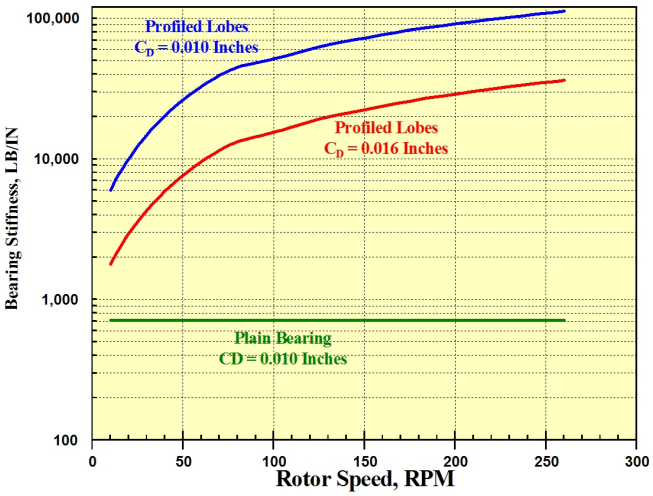

Figure 8. Stiffness Comparison Plain Versus Profiled Lobes.

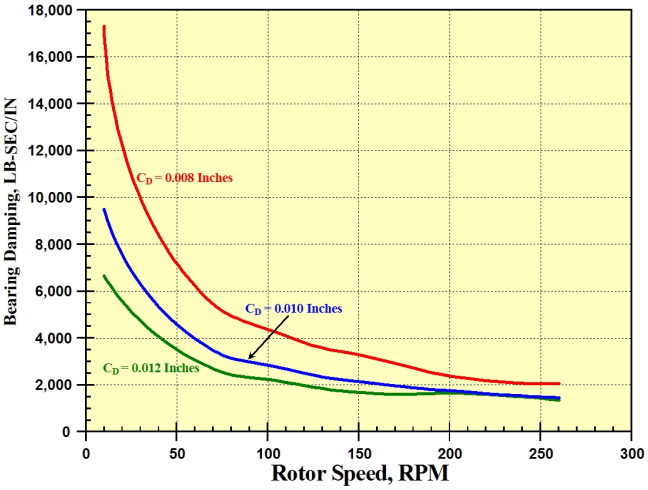

Figure 7. Plain Bearing Damping Versus Speed and Clearance.

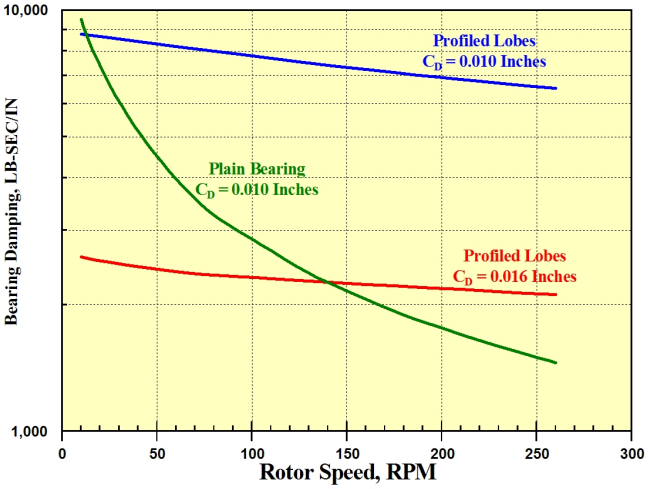

Figure 9. Damping Comparison Plain Versus Profiled Lobes.

oil is forced into the converging section, there is a pressure buildup that creates stiffness and damping. As the film diverges toward the trailing edge, the reduction in pressure helps draw the oil out to be replaced by fresh oil and keep temperatures down. From a practical standpoint, the leading and trailing edges of each pad (there are six in this bearing) have a greater clearance than the center of the pad. The pads must be symmetrical to accommodate reverse rotation.

For the new design, the diametral center-of-pad clearance will range from *10 mils to 16 mils*. The diametral edge-of-pad clearance will be greater than the center-of-pad clearance by *3 to 4 mils* using these specifications. This corresponds to a 68 to 75 percent preload. Figure 8 compares the stiffness of the original plain bearing at 10 mils clearance with the new design at its clearance extremes.

It is clear that the profiled bearing design produces significant stiffness. At equal clearance and at operating speed, the new design is 158 times stiffer than the plain bearing.

Figure 9 compares the damping produced by the original bearing at 10 mils clearance versus the damping produced by the profiled lobe bearing design as a function of speed.

The damping produced by the new design is higher than the plain bearing at 10 mils diametral clearance. At the maximum clearance of the profiled design, the damping remains higher at speeds above 138 rpm. Thus, at operating speed the profiled bearing is much more capable of controlling rotor motion than the plain bearing. Only at very low speeds is the plain bearing damping superior. This was a concern since this motor must transition from minus 250 rpm to plus 257 rpm every time it starts. To address the concern, a startup was captured on digital tape and a special high speed sampling routine was developed to track the centerline position of the shaft in the bearing during the transition. These data are only available for the new design bearing.

Figure 10 is the startup plot showing centerline position. The shaft starts out orbiting counterclockwise at 250 rpm. When the motor is energized there is a 0.6 mil jump and the shaft starts orbiting clockwise as it accelerates up to the 257 rpm synchronous speed. These data alleviated concerns that the profiled design bearing would not be able to adequately control the zero speed transition.

Rotordynamics

Initially, only the motor rotor was modeled as shown in Figure 11. This is a finite element model complete with the effects of the mass and stiffness of the motor casing. There are two rigid body modes for this machine as shown in figures 12 and 13. Both of these are critically damped and do not significantly affect the synchronous vibration. An unbalance response analysis was also conducted. This showed no resonances of any kind regardless of which bearing design was used. However, the profiled bearing managed to control rotor amplitude better than the plain design. For a given imbalance at the rotor center to excite the first mode and at the ends to excite the second mode, the amplitude at operating speed is 24 percent less at the lower bearing location with the new design.

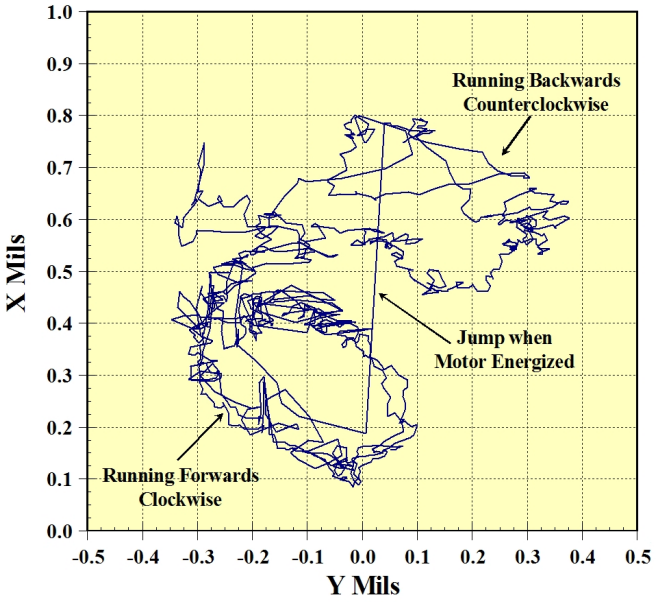

Figure 10. Startup Shaft Centerline Position with Profiled Bearing.

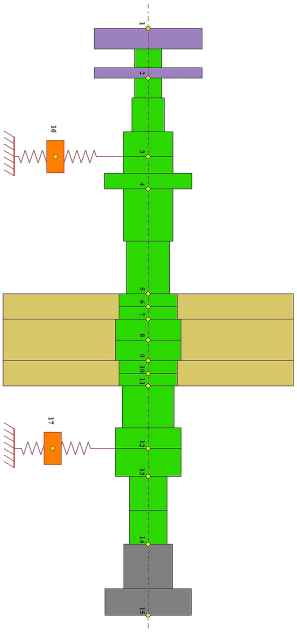

Figure 11. Finite Element Model of Motor Rotor.

FINITE ELEMENT ANALYSIS OF MOTOR STRUCTURE

Even though the failures had been eliminated with the bearing redesign, the actual failure mode had not been adequately explained by the lubrication analysis. It was still a mystery why the bearings only failed in the top half. Many people suspected that the sudden drop in ambient temperature was causing the motor frame to contract, squeezing the bearing. Figure 2 shows that the motor frame is attached to the top of the bearing and, if the frame contracted, it would pinch only at the top. These motors typically operate with a motor load of about 2500 hp. Thermal data were provided for one of the motors operating under load with an ambient temperature of 94°F. The air temperature at the inlet filters was found to be at 97°F with an average flow rate of about 5.6 ft/sec across the inlet filters. The outlet temperature was found to be 172°F, with an average flow rate of about 4.6 ft/sec.

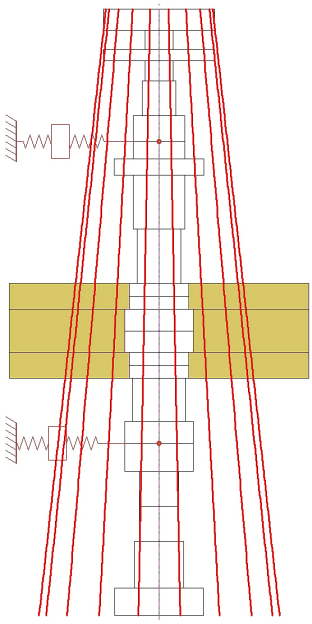

Figure 12. First Rigid Body Critical Speed of Motor Rotor.

The temperature response of these motors indicates that the bearing temperature follows ambient temperature, i.e., the bearing metal temperature drops approximately 3°F for each 4°F ambient temperature change. This bearing temperature change is similar to other electric motor bearings that are cooled with ambient air. Operating temperature of the bearings commonly indicates a bearing metal temperature change of about 60 to 75 percent of the ambient change. Figure 14 shows plant data indicating the rate of change in lower guide bearing temperature versus ambient between 70°F and 25°F for CW2-02. The plot indicates that there is a somewhat typical drop in temperature until the ambient temperature reaches about 30°F. At this point, the bearing temperature is observed to increase with additional temperature drop until the point where the temperature begins to rise for constant ambient temperature.

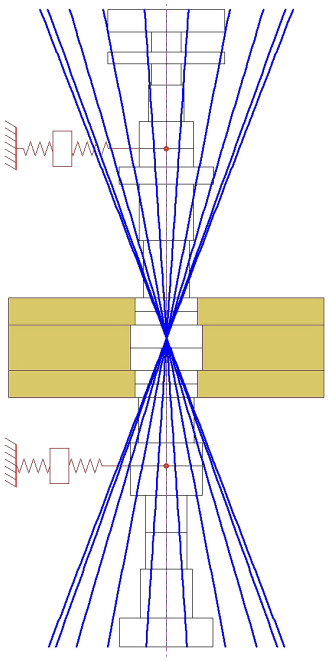

Figure 13. Second Rigid Body Critical Speed of Motor Rotor.

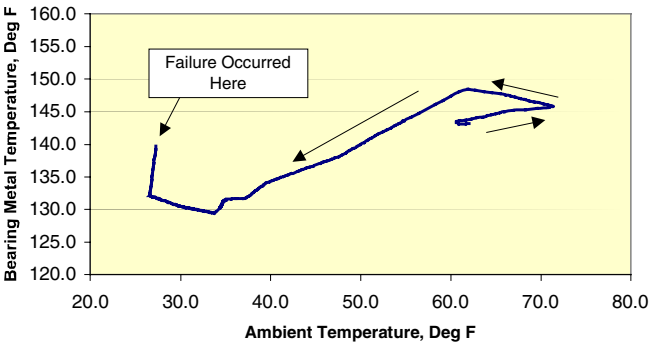

Figure 14. CW2-02 Temperature Data for Motor Lower Guide Bearing.

Figure 14 does not show the final indicated temperature of 300°F when it was shut down. The other two bearing failures showed nearly identical trends. The rise in temperature observed while the temperature drops below about 35°F suggests that some mechanism is acting to produce more heat in the bearing for lower ambient temperatures. Failure occurred at about 27°F ambient temperature. The thermal analysis was very complex and only a few of the results are shown in this paper. The finite element analysis of the bearing housing and case model is shown in Figure 15.

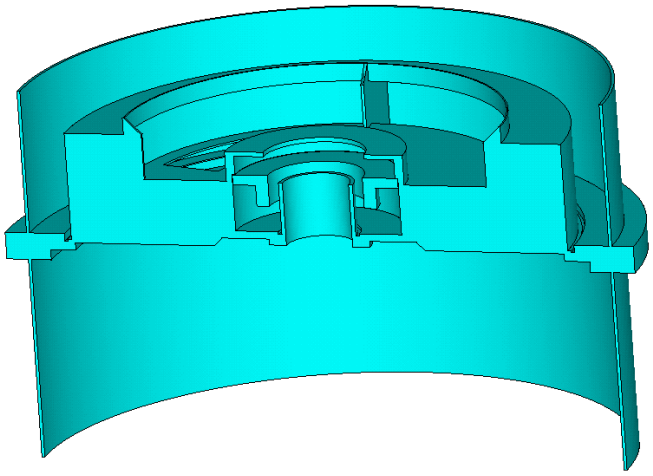

Figure 15. Finite Element Model of Motor Bearing Structure.

The boundary conditions were set based on field measurements and known conditions. Those thermal boundary conditions applied to the motor support included convection and heat flux at the bearing surface. A temperature profile at various steady-state temperatures was calculated. The heat generated at the bearing surface was selected for each iteration using the heat flow data based on the calculated bearing diametral clearance. The clearance in general was found to decrease at the top of the bearing with decreasing ambient temperature, which required input of a higher heat flux as the temperature dropped.

The thermal inertia of the motor will result in a time lag during a sudden drop in ambient temperature. The effect of this sudden time lag was modeled using a heat balance method. An effective thermal mass of 15,000 lb was used, or about 40 percent of the total stator and rotor weight. This assumption was used to estimate the amount of metal in the motor that is actually hot during operation. Using this amount of thermal inertia and the cooling characteristics of the airflow, the motor outlet air temperature was found to lag behind the ambient drop by approximately 1½ hours. Plant operating data indicate that this estimate reasonably duplicates the observed operation of the motor.

Starting with a motor assembled at 70°F and a constant bearing clearance of 8 mils on diameter, the ambient was dropped to 60°F. Figure 16 shows the deformed shape at this temperature.

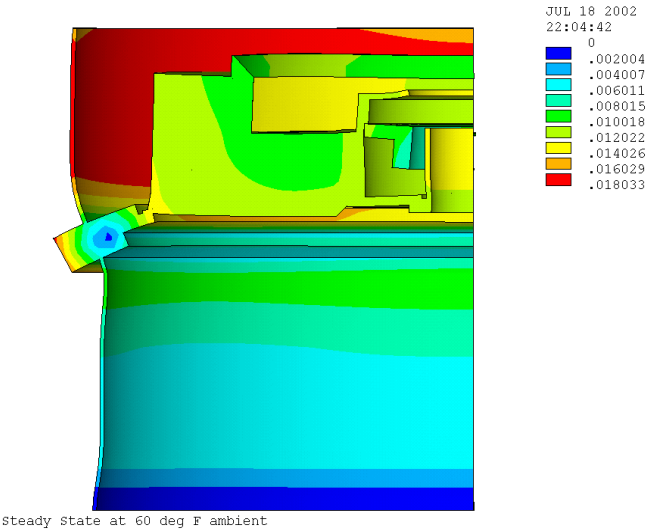

Figure 16. Motor Housing Deformation at 60 F.

The thermal distortion has caused the top of the bearing to tilt inward resulting in a top clearance of 6.4 mils and a bottom clearance of 9.4 mils. As the temperature continues to drop to 35°F, the average clearance at the top decreases to 4.6 mils as shown in Figure 17 with a transient minimum clearance of 3.9 mils. With the temperature profile at 25°F, Figure 18 shows the gradients in the motor structure.

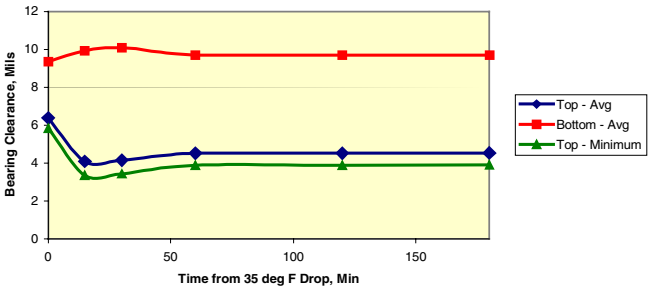

Figure 17. Sudden Ambient Temperature Effect on Bearing Clearance.

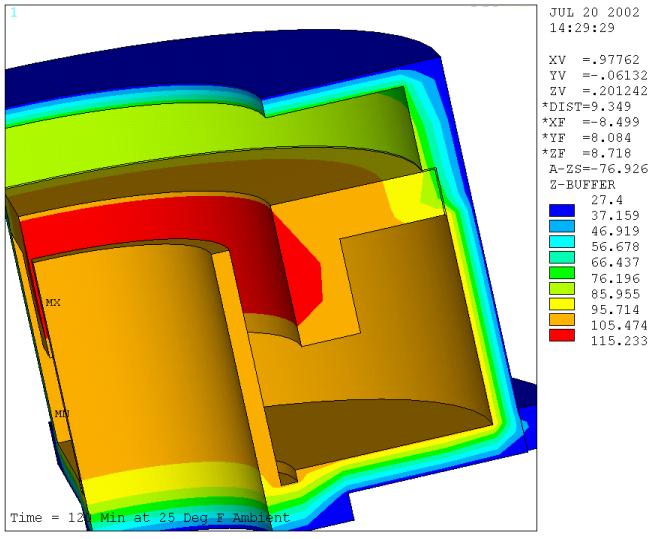

Figure 18. Temperature Profile at 25°F.

CONCLUSIONS

Three lower motor bearing failures were investigated. A modified bearing geometry was devised that provided better stiffness and damping support for the rotor. This design started out with up to twice the clearance of the original design and is more tolerant of clearance reduction due to ambient temperature changes.

The lubrication system was found to be adequate. Additional care was taken to assure that the pumping tubes were properly aligned with the oil feed groove and that the oil was properly maintained. Additional external heating during cold front passage was also used to prevent failures of plain bearings with tight clearances.

The motor has no critical speeds of concern. The predicted synchronous vibration amplitudes were reduced by 24 percent with the new bearing design. The new bearing design also reduced the measured bearing operating temperature by 10°F to 12°F.

A finite element analysis of the motor case and bearing housing revealed that reduced ambient temperature was pinching the top of the bearing by as much as 4 mils, reducing the clearance to the point where a rub was initiated and the bearing failed. Since replacing the plain bearings with the profiled design there have been no failures and all eight units survived many exposures to low ambient temperatures.

APPENDIX A

Assumptions used in the finite element analysis were:

Free Surface Model

- Model is reasonably circumferentially consistent and valid to be modeled using a two dimensional axisymmetric model.
- Oil flow into oil ports from the sump can be modeled as an equivalent flow with a flow rate reduced by the model flow area and the actual port size. The inlet flow rate was manually iterated between the 3D flow into the bearing liner and the 2D sump model.
- Portions of the sump including stationary boundaries were modeled as nonslipping surfaces (zero velocity at surface).
- Portions of the sump that were rotating were modeled as rotating with the fluid velocity equivalent to the surface velocity at the surface interface.
- Oil temperature was assumed to be constant for the entire model.
- The oil surface was assessed using the calculated volume fraction for the oil/air mixture, where areas with predicted volume fraction much less than 1.0 were assumed to be potentially foamy. A volume fraction of 0.95 was selected as a threshold for allowing the potential of foam ingestion into the bearing liner.

3D Model

- Portions of the sump including stationary boundaries were modeled as nonslipping surfaces (zero velocity at surface).
- Portions of the sump that were rotating were modeled as rotating with the fluid velocity equivalent to the surface velocity at the surface interface.

BIBLIOGRAPHY

CFX User Guide, Release 5.0, 2002, AEA Technology.

Oosthuizen, P. H. and Carscallen, W. E., 1997, *Compressible Fluid Flow*, New York, New York: McGraw-Hill.

Paterson, A. R., 1983, *A First Course in Fluid Dynamics*, Cambridge, England: Cambridge University Press.

Tullis, J. P., 1989, *Hydraulics of Pipelines*, New York, New York: John Wiley & Sons.

Wang, Y., Simmons, K., Hibberd, S., Eastwick, C., and Care, I., 2001, "*Application of CFD to Modeling Two Phase Flow in a High Speed Aero Engine Transmission Chamber*," ASME Paper FEDSM2001-18167.

ACKNOWLEDGEMENTS

The authors wish to acknowledge the contribution, support, and encouragement of Bernie Herbage and John Whalen of TCE. In addition, they would like to thank John W. Silcott of Celanese Chemical who was the monitor for this paper.